J. Phys. B: At. Mol. Opt. Phys. **30** (1997) 1013–1026. Printed in the UK PII: S0953-4075(97)79666-4

State- and isotope-dependent charge transfer of N^{4+} with atomic hydrogen in astrophysical and fusion plasmas

P C Stancil†§, B Zygelman†‖, N J Clarke‡¶ and D L Cooper‡+

† W M Keck Laboratory for Computational Physics, Department of Physics, University of Nevada, Las Vegas, NV 89154-4002, USA

‡ Department of Chemistry, University of Liverpool, PO Box 147, Liverpool L69 3BX, UK

Received 19 November 1996

Abstract. State- and target-isotope-dependent cross sections for electron capture in collisions of $N^{4+}(2s)$ with H(1s), D(1s), and T(1s) are presented for the energy range 0.01–6000 eV amu^{-1}. Results are given for capture via radial coupling into the N^{3+} $2s3s\,^1S$, $2s3p\,^1P^o$, $2s3d\,^1D$, $2s3s\,^3S$, $2s3p\,^3P^o$, $2s3d\,^3D$, and $2p3s\,^3P^o$ states and are obtained through a close-coupled, quantum-mechanical, molecular-orbital method. Fully *ab initio* molecular data determined with the spin-coupled valence-bond method are incorporated. Rate coefficients for temperatures between 1000 and 10^6 K are also presented. Applications to astrophysical environments and laboratory plasmas are addressed. The importance of state-dependent parameters for the modelling of nebulae emission lines and for fusion plasma impurity diagnostics and the potential significance of isotope effects to models of the edge region of a tokamak device are briefly discussed.

1. Introduction

Electron capture in collisions of N^{4+} with atomic hydrogen has been theoretically investigated by a number of authors at various levels of sophistication. A two-state Landau–Zener calculation was performed by Butler and Dalgarno (1980). The collision dynamics has been treated quantum mechanically by Feickert *et al* (1984), Shimakura *et al* (1992), and Zygelman *et al* (1992, 1997). The molecular orbitals (MO) of Feickert *et al* (1984) were determined by a single-configuration self-consistent-field (SCF) calculation with the so-called improved virtual orbital approach while Shimakura *et al* (1992) used a modified multiconfiguration valence-bond configuration-interaction (CI) method with a pseudopotential to describe the N^{5+} core and Zygelman *et al* (1992, 1997) performed a multiconfiguration spin-coupled valence-bond CI calculation. In addition, the calculation of Shimakura *et al* (1992) included electron translation factors. While the total cross sections of Shimakura *et al* (1992) and Zygelman *et al* (1992, 1997) are in excellent agreement with the merged-beams experiment of Huq *et al* (1989) below about 30 eV amu^{-1} and both sets of calculated state-dependent cross sections agree well with the measurements of McCullough *et al* (1995) between 290 and 1700 eV amu^{-1}, unfortunately low energy measurements of state-dependent cross sections are currently unavailable which could provide discrimination between the various theoretical approaches.

§ E-mail address: stancil@physics.unlv.edu
‖ E-mail address: bernard@physics.unlv.edu
¶ E-mail address: nickc@tc.bham.ac.uk
+ E-mail address: dlc@rs2.ch.liv.ac.uk

0953-4075/97/041013+14$19.50

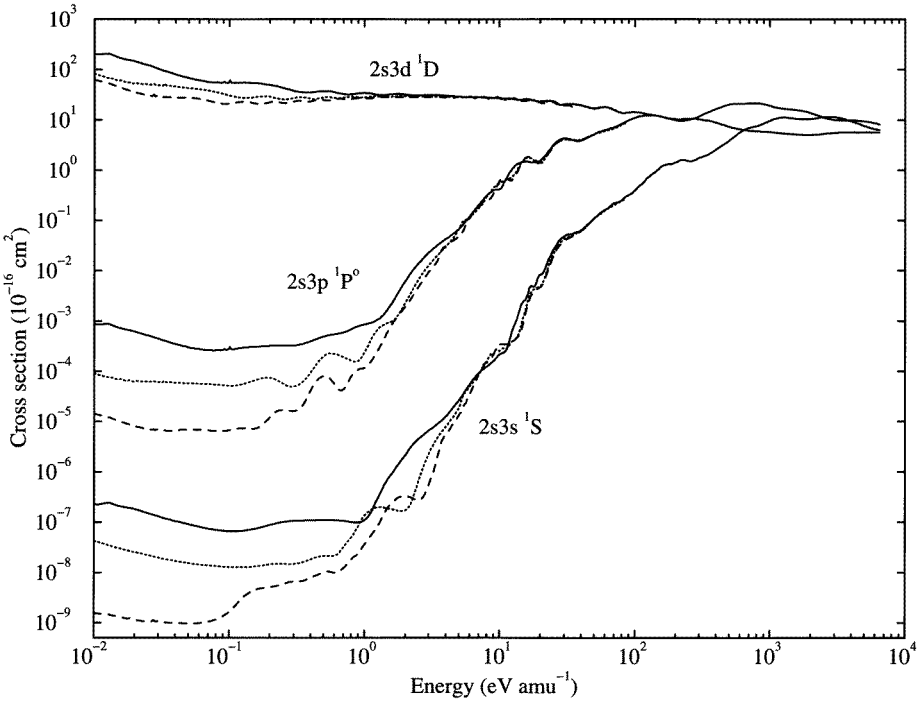

Figure 1. State- and isotope-dependent charge-transfer cross sections for the $^1\Sigma^+$ manifold of $N^{4+} + H(D, T) \rightarrow N^{3+} + H^+(D^+, T^+)$. The target H is given by the full curves, D by the dotted curves, and T by the broken curves.

The recent measurements (Folkerts *et al* 1995) of charge transfer in collisions of N^{4+} with deuterium (D) motivated us to investigate target isotope effects. In Stancil and Zygelman (1995), a significant reduction of the D target cross section in comparison to the H target was shown to occur in the $^1\Sigma^+$-manifold for energies less than about 10 eV amu^{-1}. While for this system an isotope effect is difficult to resolve in measurements of the total cross section, it is important in the determination of the state-dependent rate coefficients.

In this paper, we give detailed theoretical predications for state-dependent electron capture in collisions of N^{4+}(2s) with H, D, and tritium (T). The cross sections and rates are presented in section 2. In section 3, we discuss applications of the state-dependent rate coefficients to various astrophysical and laboratory plasmas.

2. Cross sections and rate coefficients

The fully quantal, close-coupled, molecular-orbital approach for calculating the state-dependent cross sections has been previously described (Zygelman *et al* 1992, 1997) and will not be repeated here. The *ab initio* adiabatic potentials and nonadiabatic radial couplings were given in Zygelman *et al* (1992, 1997). Four $^1\Sigma^+$ and five $^3\Sigma^+$ states were included, but rotational coupling and electron translation effects were neglected as they are expected to become important only for energies $\gtrsim$100 eV amu^{-1}. The scattering computations presented here include an energy grid of greater than 20 points per decade. Figures 1 and 2 display the state- and isotope-dependent cross sections for the $^1\Sigma^+$- and $^3\Sigma^+$-manifolds, respectively. The H target cross sections were given previously in Zygelman *et al* (1992, 1997). All data presented in this paper can be obtained via electronic mail.

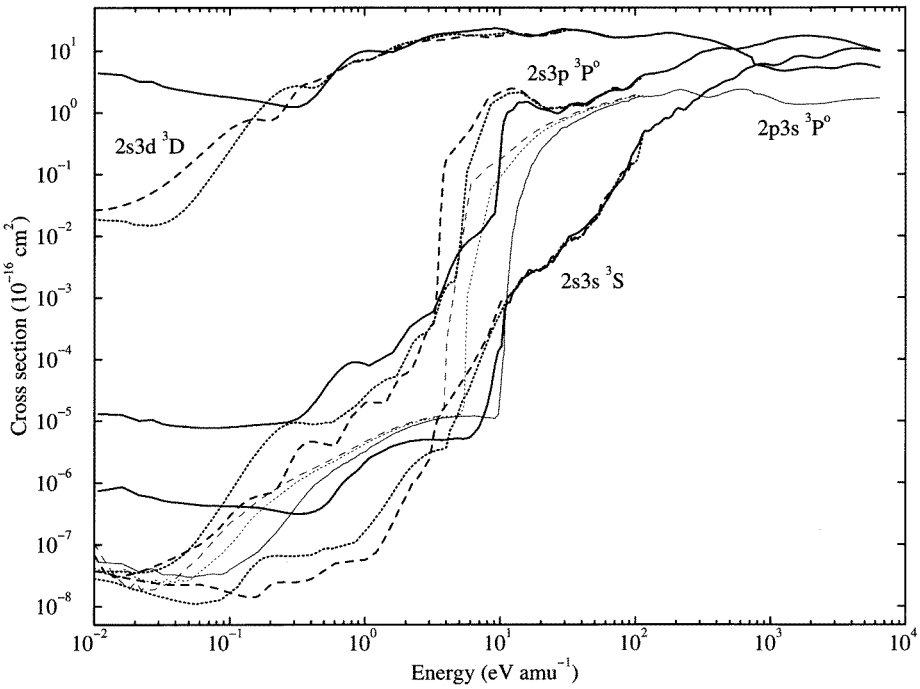

Figure 2. Same as figure 1, but for the $^3\Sigma^+$-manifold.

For collision energies $\lesssim$100 eV amu^{-1}, the $^1\Sigma^+$-manifold is dominated by capture into the N^{3+} 2s3d ^{1}D state. The rise in the 2s3d ^{1}D cross section with decreasing energy is due to an ion-induced dipole interaction. The low energy increase has been observed in several multicharged systems including the isoelectronic $O^{5+} + H \rightarrow O^{4+}(2s4p) + H^+$ reaction investigated theoretically by Gargaud (1987) and experimentally by Havener *et al* (1989). Conversely, Shimakura *et al* (1992) found that the 2s3d ^{1}D cross section decreases with decreasing energy $\lesssim$50 eV amu^{-1} (see Zygelman *et al* 1997 for a detailed comparison of cross sections). A two-state Landau–Zener analysis suggests that the low-energy behaviour of the cross sections is sensitive to the adiabatic potential energy splitting, $\Delta U(R_*)$, of the entrance and exit channels and the magnitude of the nonadiabatic radial coupling, $A_{12}(R_*)$, at the avoided crossing R_*. The values of $\Delta U(R_*)$ and $A_{12}(R_*)$ calculated by Shimakura *et al* (1992) are 18% larger and 50% smaller, respectively, than obtained by Zygelman *et al* (1992).

For energies $\lesssim$5 eV amu^{-1}, differences in the target isotope-dependent cross sections for capture into the 2s3d ^{1}D become apparent (see also figure 5). For a given mass-scaled collision energy, the cross sections decrease with increasing system-reduced mass. The same trend was predicted by Havener *et al* (1991) for collisions of O^{5+} with H and D using the Landau–Zener approximation. For captures into the 2s3s ^{1}S and 2s3p ^{1}P^o the situation is not as clear as the cross sections decrease rapidly with decreasing energy, but the reduced-mass dependence generally holds. Above $\sim$50 eV amu^{-1}, cross sections for the different target isotopes are identical.

In order to investigate further the isotope effect, we present in figure 3 partial cross sections, σ_J, as a function of angular momentum, J, for capture into the 2s3d ^{1}D for H, D, and T targets. Figure 3(*a*) shows the σ_J distribution for the low collision energy

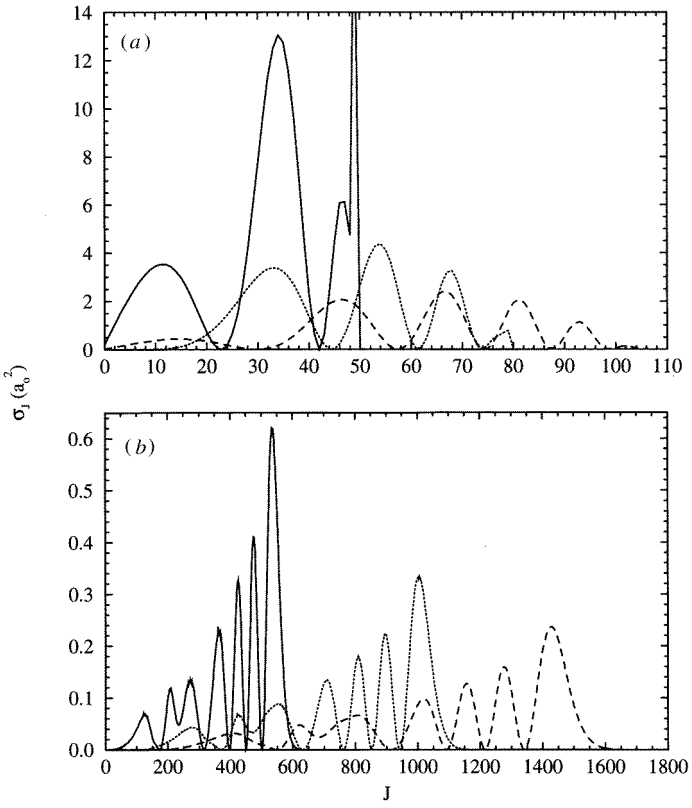

Figure 3. Partial cross sections σ_J versus J for capture into $N^{3+}(2s3d\,^1D)$ from $N^{4+} + H$ (full curves), $N^{4+} + D$ (dotted curves), and $N^{4+} + T$ (broken curves). (*a*) $E = 0.1$ eV amu^{-1}, (*b*) $E = 40$ eV amu^{-1}.

of 0.1 eV amu^{-1} where the enhancement in the total H cross section results from the proportionately larger peak in the σ_J distribution near $J = 34$ compared to D and T. For the larger collision energy of 40 eV amu^{-1} given in figure 3(*b*), σ_J increases with decreasing target mass, but the range of J increases with mass giving the net result that the total cross section is target-mass-independent. This partial cross section behaviour has been noted for the $Si^{4+} + {}^4He$ (^3He) system by Stancil *et al* (1997). The same discussion can be applied to the partial cross sections, σ_J, for capture into the $2s3d\,^3D$ as shown in figure 4.

The collision energy of 0.1 eV amu^{-1} is very near a resonance (0.1007 eV amu^{-1}) as is evident by the sharp peak in the partial cross section at $J = 49$ for H in figure 3(*a*). The feature is an orbiting resonance due to a quasibound rotational–vibrational level of the quasimolecule in the incoming channel. Theoretically these features have been found in a number of collision systems (cf Shimakura and Kimura 1991), but have eluded experimental verification. Orbiting resonances are also present at 0.033 eV amu^{-1} ($J = 59$) and 0.026 eV amu^{-1} ($J = 73$) for D and T targets, respectively. No resonances were found in the $^3\Sigma^+$-manifold.

As can be seen in figure 2, charge transfer in the $^3\Sigma^+$-manifold is considerably more complicated since the state-dependent cross sections all generally decrease with decreasing energy. Capture into the $2s3d\,^3D$ level decreases with decreasing energy because $\Delta U(R_*)$ and $A_{12}(R_*)$ are 50% larger and 44% smaller, respectively, in comparison with capture into

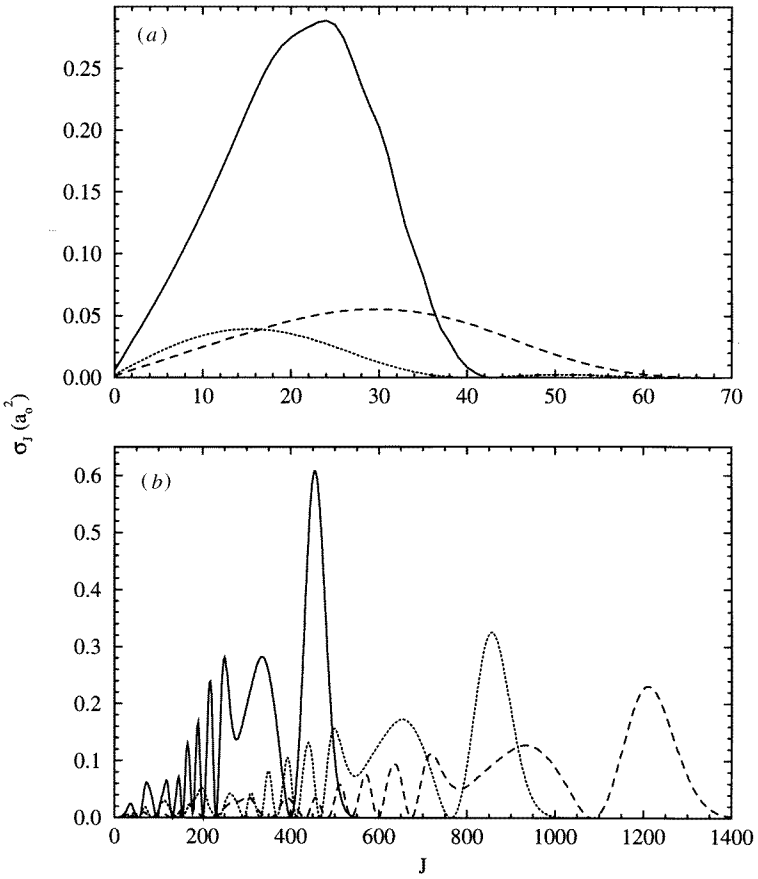

Figure 4. Same as figure 3, but for capture into $N^{3+}(2s3d\,^3D)$.

the $2s3d\,^1D$ as discussed above. The target isotope dependence appears to vary randomly with collision energy.

Figure 5 displays total isotope-dependent cross sections for the $^1\Sigma^+$- and $^3\Sigma^+$-manifolds as well as the spin-degenerate averaged sum (total). Above 50 eV amu^{-1} there is no isotope dependence in any of the cross sections. In the $^1\Sigma^+$-manifold, the rise at low energy and decrease with increasing reduced mass is evident. The isotope-dependence of the $^3\Sigma^+$-manifold as well as the spin-degenerate averaged sum for energies $\gtrsim$0.1 eV amu^{-1} is negligible in light of current experimental uncertainties. Between 1 and 30 eV amu^{-1}, the total theoretical cross sections are in good agreement with measurements and with state-selective experiments between 290 and 1700 eV amu^{-1} (cf Stancil and Zygelman 1995, Zygelman *et al* 1997). We estimate the uncertainty in the computed state-dependent cross sections to be $\sim \pm 20\%$ for capture into the $2s3d\,^1D$ and $2s3d\,^3D$. The other cross sections should be reliable to within an order of magnitude with the least accurate being the $2p3s\,^3P^o$. Below 0.1 eV amu^{-1}, the total H target cross section rises steeply with decreasing energy due to the dominance of the $^1\Sigma^+$-manifold. The D and T target cross sections also increase with decreasing energy, though not as pronounced, but the isotope-dependence is seen to be enhanced with decreasing energy suggesting the possibility for future experiments to observe an isotope effect in this collision system.

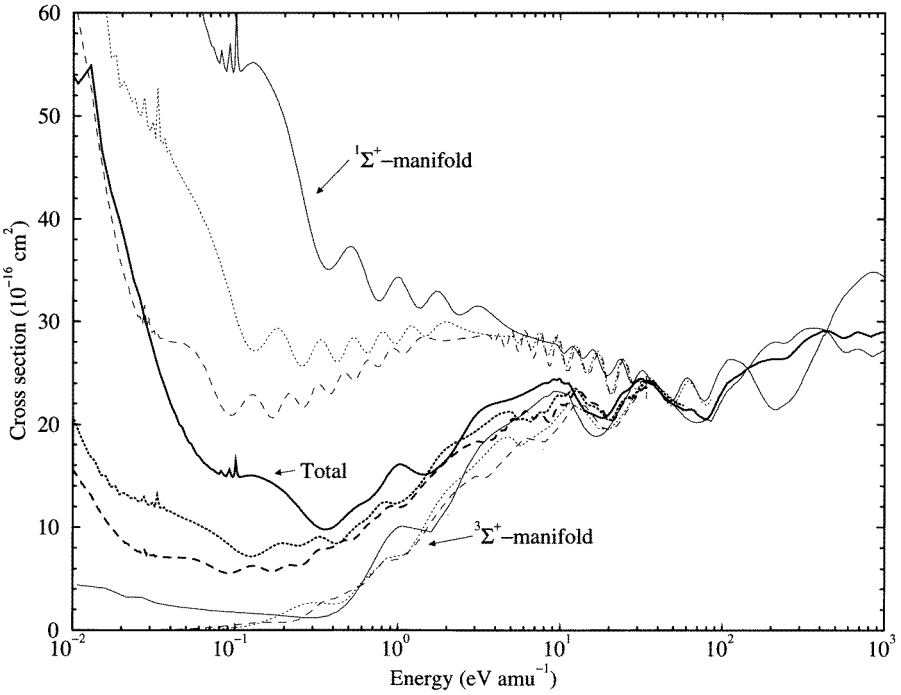

Figure 5. Total spin-dependent (light curves) and total (heavy curves) charge-transfer cross sections for $N^{4+} + H(D, T) \rightarrow N^{3+} + H^+(D^+, T^+)$. The isotope-dependent designations are the same as given in figure 1.

In tables 1, 2, and 3, we present state-dependent rate coefficients for electron capture in collisions of N^{4+} with H, D, and T, respectively, which were determined by averaging over the cross sections with a Maxwellian velocity distribution. The rates are fit to the parametric form

$$\alpha(T) = \sum_{i=1}^{2} a_i \left(\frac{T}{10\,000}\right)^{b_i} \exp\left(\frac{-T}{c_i}\right) \tag{1}$$

with the parameters a_i (cm^3 s^{-1}), b_i, and c_i (K) given in the tables. The fits are reliable to within 50% over the temperature range 1000–100 000 K except for the fit to the total which has an accuracy greater than 10%. figure 6 displays the total rate coefficients in the $^1\Sigma^+$ manifold for H, D, and T targets (note that the state-dependent rate coefficients in tables 1, 2, and 3 and figure 6 are not spin-statistically weighted). In addition, rate coefficients are also presented for the D and T targets, but obtained from the H target cross section by scaling the collision energy with the reduced masses. The scaled rate coefficients approach the actual rate coefficients at high temperatures since the cross sections are identical at high collision velocities, but figure 6 shows that the scaled rate coefficients are a factor of 1.7 and 2.4 too large at $T = 1000$ K for the D and T targets, respectively.

Table 4 presents a comparison of rate coefficients to previous calculations. For the $^1\Sigma^+$-manifold, the current results have the same temperature dependence as given by the quantal computations of Feickert *et al* (1984), but the present coefficients are typically 25–40% larger. The new rates are also 10–100 times larger than the Landau–Zener calculations of Butler and Dalgarno (1980). Following the same procedures for modelling the diabatic

Table 1. State-dependent and total spin-averaged rate coefficients α ($cm^3\ s^{-1}$) as a function of temperature T for $N^{4+} + H \rightarrow N^{3+} + H^+$. The state-dependent values do not include the spin-degeneracy factors $\frac{1}{4}$ and $\frac{3}{4}$ for singlets and triplets, respectively, while the total equals $\frac{1}{4}\alpha(^1\Sigma^+) + \frac{3}{4}\alpha(^3\Sigma^+)$. Fitting parameters a_i ($cm^3\ s^{-1}$), b_i, and c_i (K) according to equation (1) are given at the end of the table.

	$^1\Sigma^+$			$^3\Sigma^+$				
T (K)	2s3s	2s3p	2s3d	2s3s	2s3p	2s3d	2p3s	Total
1 000	4.3−18[a]	1.6−14	2.6−9	1.9−17	5.2−16	8.5−11	1.0−17	7.2−10
2 000	7.0−18	2.8−14	3.0−9	3.8−17	1.7−15	1.9−10	5.4−17	8.8−10
4 000	2.9−17	1.0−13	3.6−9	1.3−16	6.3−15	5.3−10	2.1−16	1.3−9
6 000	1.1−16	3.6−13	4.1−9	2.6−16	1.7−14	9.0−10	4.3−16	1.7−9
8 000	3.0−16	9.1−13	4.6−9	3.8−16	4.5−14	1.3−9	6.7−16	2.1−9
10 000	6.4−16	1.9−12	5.0−9	5.4−16	1.2−13	1.6−9	1.0−15	2.5−9
20 000	9.5−15	1.7−11	6.6−9	8.9−15	6.7−12	3.3−9	1.3−13	4.2−9
40 000	3.1−13	1.2−10	8.6−9	1.5−13	8.6−11	5.7−9	6.4−12	6.5−9
60 000	1.7−12	3.1−10	1.0−8	4.9−13	2.0−10	7.2−9	2.8−11	8.2−9
80 000	4.6−12	5.6−10	1.1−8	1.1−12	3.1−10	8.4−9	6.6−11	9.5−9
100 000	9.0−12	8.5−10	1.2−8	2.1−12	4.2−10	9.5−9	1.1−10	1.1−8
200 000	5.8−11	2.6−9	1.4−8	2.1−11	9.6−10	1.3−8	4.2−10	1.5−8
400 000	3.1−10	6.5−9	1.6−8	1.8−10	2.3−9	1.8−8	1.1−9	2.2−8
600 000	7.0−10	9.9−9	1.8−8	4.9−10	4.0−9	2.1−8	1.7−9	2.8−8
800 000	1.2−9	1.3−8	1.9−8	9.2−10	5.9−9	2.4−8	2.2−9	3.3−8
1 000 000	1.7−9	1.6−8	1.9−8	1.4−9	7.9−9	2.6−8	2.6−9	3.8−8
a_1	7.3−16	1.8−12	4.5−9	2.1−15	1.9−13	4.6−10	2.9−14	2.5−9
b_1	4.2	3.0	4.5−1	2.0	5.0	1.1	3.3	6.5−1
c_1	1.7+5	1.3+5	1.0+6	3.1+3	2.7+4	7.8+5	2.2+3	2.9+6
a_2	2.7−17	1.0−12	5.0−10	6.7−16	2.5−13	1.4−9	1.7−15	3.2−8
b_2	8.6−1	1.5	−1.6−1	3.7	2.5	1.4	6.7	9.6−1
c_2	7.3+4	1.4+3	−3.3+5	4.3+5	2.3+3	4.1+4	2.4+4	3.3+2

[a] The notation 4.3−18 corresponds to 4.3×10^{-18}.

potentials as Butler and Dalgarno, we obtain Landau–Zener rates which are in much better agreement with our quantal results. The empirical potentials give $R_* = 7.47\ a_0$ for the potential correlating asymptotically to the 2s3d ^{1}D. The *ab initio* result is $R_* = 8.25\ a_0$.

Coefficients for the $^3\Sigma^+$-manifold deviate significantly from the Feickert *et al* (1984) values due to the different behaviour of the cross sections at low energy. While our $^3\Sigma^+$ cross sections decrease with decreasing energy for $E > 0.3$ eV amu^{-1}, Feickert *et al*'s rise, so that their rates are overestimated for $T \lesssim 10\,000$ K.

3. Applications

3.1. Astrophysical plasmas

Multiply charged ions of nitrogen are abundant in many astronomical environments. N IV and N V lines are observed in the galactic halo (Pettini and West 1982, Savage and Massa 1985), planetary nebulae (Clegg *et al* 1987), quasars (Osterbrock 1989), hot stellar winds (Guinan and Sion 1982), novae (Morisset and Péquignot 1996), and other illuminated gaseous nebulae. Péquignot *et al* (1978) demonstrated that charge transfer must be included in models of planetary nebulae to accurately explain the ionization structure. Once the

Table 2. State-dependent and total spin-averaged rate coefficients α (cm^3 s^{-1}) as a function of temperature T for $N^{4+} + D \rightarrow N^{3+} + D^+$. The state-dependent values do not include the spin-degeneracy factors $\frac{1}{4}$ and $\frac{3}{4}$ for singlets and triplets, respectively, while the total equals $\frac{1}{4}\alpha(^1\Sigma^+) + \frac{3}{4}\alpha(^3\Sigma^+)$. Fitting parameters a_i (cm^3 s^{-1}), b_i, and c_i (K) according to equation (1) are given at the end of the table.

	$^1\Sigma^+$			$^3\Sigma^+$				
T(K)	2s3s	2s3p	2s3d	2s3s	2s3p	2s3d	2p3s	Total
1 000	5.4−19[a]	2.1−15	1.3−9	9.0−19	5.3−17	1.6−11	5.8−18	3.3−10
2 000	7.7−19	3.5−15	1.5−9	2.2−18	2.2−16	6.8−11	2.7−17	4.4−10
4 000	1.9−18	8.7−15	2.0−9	5.3−18	6.2−16	2.1−10	9.8−17	6.6−10
6 000	4.5−18	2.1−14	2.4−9	1.2−17	1.3−15	3.7−10	2.0−16	8.9−10
8 000	9.8−18	5.3−14	2.8−9	2.5−17	3.0−15	5.6−10	3.2−16	1.1−9
10 000	2.2−17	1.2−13	3.2−9	4.7−17	1.0−14	7.5−10	5.5−16	1.4−9
20 000	5.5−16	1.7−12	4.5−9	6.1−16	2.0−12	1.7−9	6.8−14	2.4−9
40 000	1.1−14	2.0−11	6.3−9	1.7−14	4.9−11	3.3−9	2.6−12	4.1−9
60 000	7.8−14	6.5−11	7.6−9	7.9−14	1.5−10	4.5−9	1.1−11	5.4−9
80 000	3.3−13	1.4−10	8.6−9	2.0−13	2.5−10	5.4−9	2.7−11	6.4−9
100 000	8.9−13	2.4−10	9.4−9	3.7−13	3.4−10	6.2−9	4.8−11	7.3−9
200 000	1.0−11	9.4−10	1.2−8	3.3−12	6.5−10	9.3−9	2.0−10	1.1−8
400 000	6.7−11	2.8−9	1.4−8	3.3−11	1.2−9	1.3−8	5.6−10	1.6−8
600 000	1.8−10	4.9−9	1.6−8	1.1−10	1.8−9	1.6−8	9.2−10	1.9−8
800 000	3.5−10	7.0−9	1.7−8	2.3−10	2.6−9	1.8−8	1.3−9	2.3−8
1 000 000	5.6−10	8.8−9	1.7−8	3.9−10	3.5−9	2.0−8	1.6−9	2.6−8
a_1	2.4−17	1.4−13	3.1−9	1.1−16	2.6−14	1.5−10	1.0−14	1.4−9
b_1	4.6	3.3	5.1−1	1.9	8.0	1.4	3.1	7.5−1
c_1	2.1+5	2.0+5	1.2+6	2.5+3	1.1+4	5.5+5	2.2+3	1.6+6
a_2	3.6−18	3.6−13	4.9−11	5.6−17	2.0−14	8.0−10	9.1−16	2.9−6
b_2	8.6−1	1.9	−7.9−1	3.9	2.4	1.7	6.4	3.1
c_2	2.3+4	1.1+3	−1.3+5	4.2+5	2.4+3	3.4+4	2.8+4	3.1+2

[a] The notation 5.4−19 corresponds to 5.4×10^{-19}.

neutral hydrogen to electron density ratio exceeds $\sim10^{-3}$, recombination is dominated by charge transfer (Shields 1988).

Charge transfer may be significant for some x-ray nebulae models, for example a compact source embedded in a diffuse or dense interstellar cloud (Kallman and McCray 1982). For low-velocity shocks, Butler and Raymond (1980) have shown that the column densities of multiply charged ions are significantly reduced when charge transfer is included in the models. Baliunas and Butler (1980) pointed out the importance of charge transfer as an ionization source and demonstrated its effect on the temperature dependence of ion line emissivity peaks. This has important implications for solar and stellar atmospheric density diagnostics.

In supernova remnants, charge transfer is a crucial process in establishing the ionization and thermal balance. Gamma rays from ^{56}Co decays in the ejecta produce energetic electrons which collide with metals creating highly charged ions, but charge exchange with H tends to keep them singly ionized (Xu and McCray 1991). The lack of accurate charge transfer cross sections for many important systems has hindered the progress of modelling spectra from late-time supernovae.

In figure 7 we present spin-statistically weighted rate coefficients for capture into singlet and triplet N^{3+} states due to collisions with H. For temperatures less than 30 000 K, typical of

Table 3. State-dependent and total spin-averaged rate coefficients α ($cm^3\ s^{-1}$) as a function of temperature T for $N^{4+} + T \rightarrow N^{3+} + T^+$. The state-dependent values do not include the spin-degeneracy factors $\frac{1}{4}$ and $\frac{3}{4}$ for singlets and triplets, respectively, while the total equals $\frac{1}{4}\alpha(^1\Sigma^+) + \frac{3}{4}\alpha(^3\Sigma^+)$. Fitting parameters a_i ($cm^3\ s^{-1}$), b_i, and c_i (K) according to equation (1) are given at the end of the table.

	$^1\Sigma^+$			$^3\Sigma^+$				
T(K)	2s3s	2s3p	2s3d	2s3s	2s3p	2s3d	2p3s	Total
1 000	4.8−20[a]	2.2−16	8.2−10	6.4−19	5.8−18	8.7−12	4.2−18	2.1−10
2 000	1.3−19	4.6−16	1.0−9	8.6−19	2.9−17	3.0−11	1.8−17	2.7−10
4 000	3.6−19	1.5−15	1.4−9	1.5−18	1.4−16	1.1−10	6.3−17	4.2−10
6 000	8.8−19	3.6−15	1.7−9	2.5−18	3.3−16	2.1−10	1.2−16	5.9−10
8 000	2.0−18	8.8−15	2.0−9	4.4−18	9.5−16	3.2−10	2.0−16	7.5−10
10 000	3.9−18	2.1−14	2.3−9	8.7−18	5.5−15	4.4−10	3.7−16	9.2−10
20 000	6.6−17	3.7−13	3.5−9	2.2−16	1.0−12	1.1−9	6.2−14	1.7−9
40 000	2.2−15	5.5−12	5.1−9	5.0−15	2.5−11	2.3−9	2.2−12	3.0−9
60 000	1.3−14	2.2−11	6.3−9	2.6−14	9.0−11	3.2−9	8.5−12	4.0−9
80 000	5.3−14	5.3−11	7.2−9	7.1−14	1.8−10	4.0−9	1.9−11	4.9−9
100 000	1.6−13	9.9−11	7.9−9	1.4−13	2.6−10	4.7−9	3.2−11	5.7−9
200 000	3.1−12	4.9−10	1.0−8	1.3−12	5.7−10	7.3−9	1.3−10	8.7−9
400 000	2.6−11	1.7−9	1.3−8	1.3−11	9.1−10	1.1−8	3.5−10	1.3−8
600 000	7.8−11	3.1−9	1.4−8	4.2−11	1.3−9	1.3−8	5.9−10	1.6−8
800 000	1.6−10	4.6−9	1.5−8	9.4−11	1.7−9	1.5−8	8.3−10	1.9−8
1 000 000	2.7−10	6.1−9	1.6−8	1.7−10	2.3−9	1.7−8	1.1−9	2.1−8
a_1	2.8−18	2.5−14	1.9−9	1.6−17	1.1−14	9.3−11	7.4−15	9.3−10
b_1	4.9	3.7	4.7−1	1.3	8.0	1.5	3.1	8.2−1
c_1	2.3+5	1.8+5	2.8+5	2.7+3	1.2+4	5.4+4	2.0+3	1.4+6
a_2	1.5−18	3.0−14	5.8−10	1.1−17	1.2−14	4.4−10	5.9−16	2.1−7
b_2	1.5	1.9	8.7−1	4.2	3.2	1.8	5.9	2.3
c_2	5.3+4	1.6+3	1.3+6	3.3+5	2.4+3	3.7+4	4.2+4	3.7+2

[a] The notation 4.8−20 corresponds to 4.8×10^{-20}.

planetary nebulae (PN), capture into the 2s3d ^{1}D and ^{3}D states dominate with rate coefficients greater by a factor of $\sim$ 100 compared to capture into other channels. Emission lines at 335 and 284 Å in the extreme ultraviolet (EUV) should be the strongest and most affected by charge transfer. Coincidentally, observations of PNs in the EUV with the *Extreme Ultraviolet Explorer (EUVE)* satellite are in the initial phases (cf Fruscione *et al* 1995). It is unclear though whether emissions in the EUV are due to the central star or the extended nebula. The spectral region less than 1200 Å has yet to be modelled for PNs.

After the initial decays from charge-transfer capture states, the cascade emissions 765, 1487, and 1719 Å should be strong. The 765 Å line will be difficult to observe since it occurs near the long wavelength edge of the *EUVE* spectral range. The 1487 Å intercombination line is observed in many PNs and is an important electron density diagnostic. Clegg *et al* (1987) have modelled this line in NGC 3918 using the rate coefficients of Feickert *et al* (1984) and obtained a flux that was 13% larger than observed. Use of our new rate coefficients for capture into the 2s3d ^{3}D, which is a factor of 1.7 smaller than Feickert *et al*'s (1984) at 10 000 K, may bring the modelled and observed line flux into closer agreement. In addition, in the high-velocity shock models of Butler and Raymond (1980), they found that inclusion of charge transfer increased the 1487 Å line by only 0.5%. This model incorporated the Landau–Zener rate coefficients calculated by Butler and Dalgarno

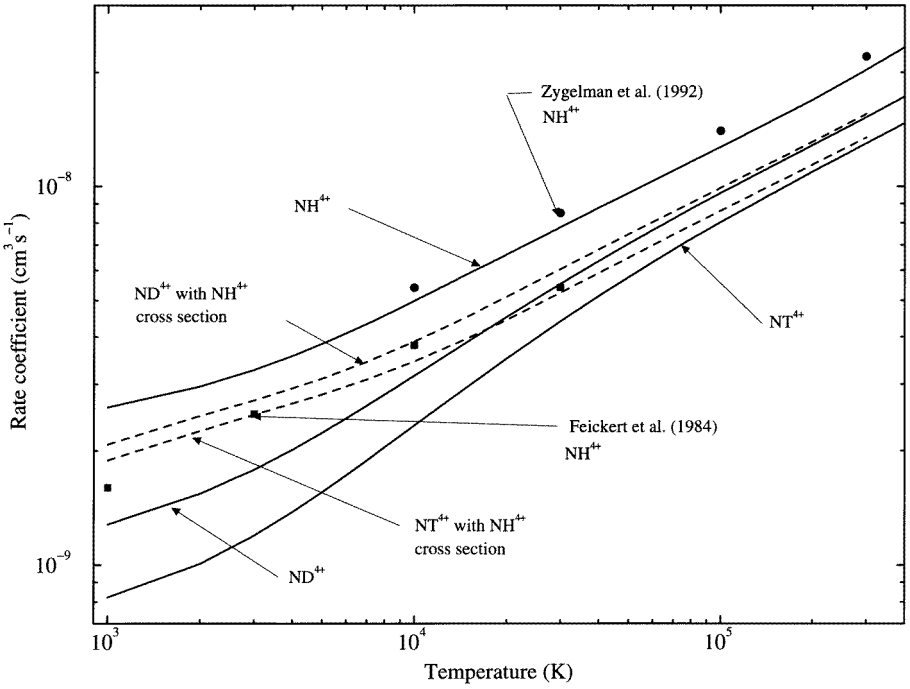

Figure 6. Isotope-dependent rate coefficients for the $^1\Sigma^+$ manifold of $N^{4+} + H(D, T) \rightarrow N^{3+} + H^+(D^+, T^+)$. Rate coefficients determined with the isotope-dependent cross section are given by the full curves, while the broken curves represent rate coefficients obtained by scaling the H target cross section.

Table 4. Comparison of rate coefficients for $N^{4+} + H \rightarrow N^{3+} + H^+$.

	T (K)				
	1000	3000	10 000	30 000	100 000
Singlets: Quantal					
This work	2.6−9[a]	3.3−9	5.0−9	7.8−9	1.3−8
Feickert *et al* (1984)	1.6−9	2.5−9	3.8−9	5.4−9	8.2−9
Singlets: Landau–Zener					
This work	3.1−10	5.7−10	1.7−9	4.4−9	9.9−9
Butler and Dalgarno (1980)	6.4−11	2.7−11	1.6−10	8.7−10	–
Triplets: Quantal					
This work	8.5−11	3.5−10	1.6−9	4.7−9	1.0−8
Feickert *et al* (1984)	9.3−10	1.3−9	2.7−9	4.6−9	7.0−9

[a] The notation 2.6−9 corresponds to 2.6×10^{-9}.

(1980) which we showed above (see table 4) to be a factor of ∼10 too small at the highest temperatures. Inclusion of our new quantal rate coefficients may enhance this effect.

The 1719 Å line is also observed in PNs, but charge transfer with H should have little effect on its intensity. Its $2p^2\,^1D$ upper state can only be populated by cascade following electron capture from H into the $2s3p\,^1P^o$ and $2p3s\,^1P^o$ which have rate coefficients

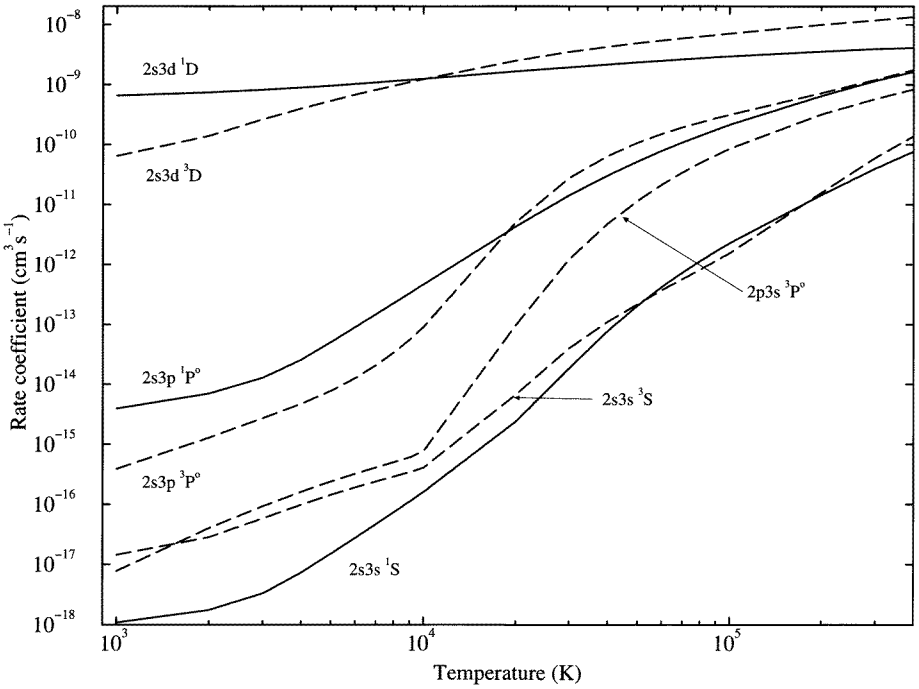

Figure 7. State-dependent rate coefficients for $N^{4+}(2s) + H(1s) \rightarrow N^{3+}(n\ell n'\ell') + H^+$. The rates are statistically weighted according to: $\alpha(^1\Sigma^+)/4$ and $3\alpha(^3\Sigma^+)/4$.

$\lesssim 10^{-12}$ cm^3 s^{-1} for $T \lesssim 10\,000$ K. Electron capture from He though can populate the the $2p^2\,{}^1D$ state with a rate coefficient estimated by Butler and Dalgarno (1980) to be 2×10^{-9} cm^3 s^{-1} using the Landau–Zener approximation (no quantal calculations of electron capture for the N^{4+} + He system exist). Charge transfer from He can also populate the $2p^2\,{}^1S$, as indicated by the 280–1700 eV amu^{-1} state-selective measurements of McLaughlin *et al* (1993), and for temperatures $\gtrsim 18\,000$ K, the $2p3s\,{}^3P^o$. It is possible that reactions with He can lead to capture into the $2p^2\,{}^3P$, but the process can only proceed by a second-order spin–orbit coupling mechanism with a rate coefficient probably $\lesssim 10^{-11}$ cm^3 s^{-1}. Charge transfer from He may therefore have some effect on the 765, 922–924, 955, 1487 and 1719 Å lines, but not on emissions at 284 and 335 Å, populated through H electron capture. The 4606 Å $5g\,{}^3G - 6h\,{}^3H^o$ recombination line is also observed in PNs, but is unaffected by charge transfer since electron capture into its lower state is endothermic by 4.593 and 15.843 eV for collisions with H and He, respectively. Detailed modelling of EUV, UV, and optical lines and in particular of those features which are influenced by charge transfer may aid in verifying the accuracy of state-dependent electron capture cross sections and provide a discriminant between the theoretical approaches. This method has proved successful for situations where the effect of charge transfer is significant enough to outweigh nebula modelling uncertainties (Shields 1988).

3.2. Fusion plasmas

Charge transfer is well established as an important fundamental atomic process in laboratory plasmas with physical conditions ranging from any combination of low-to-high density and

temperature. We will only briefly address here the possible significance of electron capture in collision of N^{4+} with neutral hydrogen in tokamak fusion devices. The discussion is applicable to other partially or fully ionized species that may be found in the tokamak plasma environment. For a more complete survey, see the recent reviews by Janev (1993, 1995).

A modern tokamak device consists of a D–T plasma heated to ∼100 keV and magnetically confined in a pressure vessel. Complicated interactions between the walls and the plasma introduce various impurities at various stages of ionization into the plasma. The plasma can be spatially divided into the central and edge regions. The fusion reactions occur in the central region. Neutral D and T may be present (unlike other discussions of fusion plasmas, we distinguish between the isotopes of hydrogen), but because the temperature is high the neutral abundance is less than $\sim 10^{-5}$ implying that charge transfer is not an important process in this region (Janev 1993).

Particle energies are significantly lower in the edge plasma which can be further partitioned into the scrap-off region, with temperatures between ∼20 and 300 eV, and the divertor chamber where the temperature ranges between ∼3 and 50 eV. As such, the edge plasma, in particular the divertor region, is characterized by a high neutral D and T abundance as well as a high impurity abundance. The neutral and impurity abundances increase with radial distance from the central plasma. The conditions of the plasma edge establish the boundary conditions of the entire plasma and therefore affect the central region where the fusion reactions occur. Charge exchange is significant in the edge region and in turn plays an important role for the realization of fusion as a viable energy source.

Charge transfer drives the edge plasma ionization balance to a situation far from coronal equilibrium. It also influences the transfer of thermalized particles in the divertor region. The high concentrations of neutral D and T and impurities in the edge region are due to a high rate of atom/ion recycling between the plasma and walls. Charge transfer, particularly for impurities A^{q+} with $q \geqslant 4$, is important for accurate modelling of the recycling process (Janev 1993).

Since many of the impurities in the edge plasma may be partially ionized, radiation from excited states results in energy loss from and cooling of the plasma. This is a severe problem for the attainment of ignition, continuation of the burn, and energy production efficiency. The problem is further amplified when electron capture is considered since for multiply charged ions capture primarily precedes to highly excited states which radiate readily in the ultraviolet. In addition, fully ionized, and therefore nonradiating, species become hydrogenlike and contribute to the impurity radiation loss. Inclusion of charge transfer may result in an increase of the impurity radiative power density by a factor of ∼30 in some models (Hogan 1983). This power loss, enhanced by charge exchange, requires higher fusion temperatures in the central region to compensate for the reduction in efficiency (Drawin 1983).

Conversely, radiative cooling is currently thought to be beneficial (Janev 1995). The majority of plasma power and high energy particle flux from the central region is directed on to a relatively small area on the divertor plates. The resulting thermal load is approximately an order of magnitude larger than current materials can withstand without significant deterioration. It is anticipated that inelastic collisional processes, such as charge transfer, may reduce the total load and spread it over a larger area. The density of ambient species and impurities may be insufficient to attain tolerable thermal loads so that some impurities, including N, may have to be introduced, in a controlled fashion, into the edge region to enhance the radiative cooling.

In all of the issues addressed above, theoretical models of the plasma environment have

incorporated, where available, charge transfer cross section and rate coefficients for H while the plasma contains D and T. The current calculations for partially ionized N^{4+} indicate a small but potentially significant reduction of the D and T $^1\Sigma^+$-manifold cross sections compared to H below a few eV. This corresponds to conditions at the very edge of the divertor region and implies that the impurity radiative power density which rises rapidly at low temperatures (Hogan 1983) may be somewhat reduced. Further, as suggested by Stancil and Zygelman (1995), this isotope effect will increase in importance as the atomic mass and degree of ionization of the impurity species increases. Common wall materials may include Si, Ti, Fe, Mo, and W. A Landau–Zener estimate for Ti^{22+} indicates that the isotope effect will be significant below a few hundred eV (Stancil and Zygelman 1995).

Finally, the current calculations may be useful for impurity abundance diagnostics. One method, called charge exchange spectroscopy (CXS), involves the injection of a neutral D beam at several keV and measurement of the resulting emissions following electron capture (see Isler 1994 for a review). Isotope effects play little role at these energies, but state-dependent cross sections are required in order to compute the impurity abundances (Post 1983). Absolute state-dependent cross sections are not easily measured in the laboratory so that theoretical computations must be relied upon. While our results extend up to only 6 keV amu^{-1}, somewhat beyond the limit of the reliability of our method, they have some utility for interpreting CXS measurements.

4. Summary

We have presented state-dependent cross sections and rate coefficients for electron capture in low-energy collisions of N^{4+} with hydrogen and its isotopes. Attention has been drawn to the possible importance of isotope effects in modelling the edge region of tokamak fusion plasmas and the use of state-dependent parameters for estimating impurity abundances in fusion plasmas and modelling emission lines in gaseous nebulae. There is still a great need for accurate quantal calculations for many lowly charged and highly charged systems for astrophysical and fusion applications, respectively.

Acknowledgments

PCS and BZ acknowledge support from NSF EPSCoR grant OSR-9353227 in Chemical Physics to the state of Nevada and the W M Keck Foundation.

References

Baliunas S L and Butler S E 1980 *Astrophys. J. Lett.* **235** L45
Butler S E and Dalgarno A 1980 *Astrophys. J.* **241** 838
Butler S E and Raymond J C 1980 *Astrophys. J.* **240** 680
Clegg R E S, Harrington J P, Barlow M J and Walsh J R 1987 *Astrophys. J.* **314** 551
Drawin H W 1983 *Atomic and Molecular Physics of Controlled Thermonuclear Fusion* ed C J Joachain and D E Post (New York: Plenum) p 341
Feickert C A, Blint R J, Surratt G T and Watson W D 1984 *Astrophys. J.* **286** 371
Folkerts L, Haque M A, Havener C C, Shimakura N and Kimura M 1995 *Phys. Rev.* A **51** 3685
Fruscione A, Drake J J, McDonald K and Malina R F 1995 *Astrophys. J.* **441** 726
Gargaud M 1987 *Doctoral Thesis* L'Université De Bordeau I
Guinan E F and Sion E M 1982 *Astrophys. J.* **258** 217
Havener C C, Huq M S, Krause H F, Schulz P A and Phaneuf R A 1989 *Phys. Rev.* A **39** 1725
Havener C C, Meyer F W and Phaneuf R A 1991 *Proc. 17 Int. Conf. on Physics of Electronic and Atomic Collisions* (Bristol: Institute of Physics) p 381

Hogan J T 1983 *Atomic and Molecular Physics of Controlled Thermonuclear Fusion* ed C J Joachain and D E Post (New York: Plenum) p 35
Huq M S, Havener C C and Phaneuf R A 1989 *Phys. Rev.* A **40** 1811
Isler R C 1994 *Plasma Phys. Control. Fusion* **36** 171
Janev R K 1993 *Review of Fundamental Processes and Applications of Atoms and Molecules* ed C D Lin (Singapore: World Scientific) p 1
Janev R K 1995 *Atomic and Molecular Processes in Fusion Edge Plasmas* ed R K Janev (New York: Plenum) p 1
Kallman T R and McCray R 1982 *Astrophys. J. Suppl.* **50** 263
McCullough R W, McLaughlin T K, Hodgkinson J M and Gilbody H B 1995 *Nucl. Instrum. Methods* B **98** 199
McLaughlin T K, Tanuma H, Hodgkinson J M, McCullough R W and Gilbody H B 1993 *J. Phys. B: At. Mol. Phys.* **26** 3871
Morisset C and Péquignot D 1996 *Astron. Astrophys.* **312** 135
Osterbrock D E 1989 *Astrophysics of Gaseous Nebulae and Active Galactic Nuclei* (Mill Valley: University Science Books)
Péquignot D, Aldrovandi S M V and Stasinska G 1978 *Astron. Astrophys.* **63** 313
Pettini M and West K A 1982 *Astrophys. J.* **260** 561
Post D E 1983 *Atomic and Molecular Physics of Controlled Thermonuclear Fusion* ed C J Joachain and D E Post (New York: Plenum) p 539
Savage B D and Massa D 1985 *Astrophys. J. Lett.* **295** L9
Shields G A 1988 *Molecular Astrophysics* ed T W Hartquist (Cambridge: Cambridge University Press) p 461
Shimakura N, Itoh M and Kimura M 1992 *Phys. Rev.* A **45** 267
Shimakura N and Kimura M 1991 *Phys. Rev.* A **44** 1659
Stancil P C and Zygelman B 1995 *Phys. Rev. Lett.* **75** 1495
Stancil P C, Zygelman B, Clarke N J and Cooper D L 1997 *Phys. Rev.* A 55 in press
Xu Y and McCray R 1991 *Supernovae* ed S E Woosley (New York: Springer) p 444
Zygelman B, Cooper D L, Ford M J, Dalgarno A, Gerratt J and Raimondi M 1992 *Phys. Rev.* A **46** 3846
Zygelman B, Stancil P C, Clarke N J and Cooper D L 1997 *Phys. Rev.* A in press